Long-Range Incommensurate Charge Fluctuations in (Y,Nd)$Ba_2Cu_3O_{6+x}$

G. Ghiringhelli *et al.*

Science **337**, 821 (2012);
DOI: 10.1126/science.1223532

13. E. Semenova *et al.*, *Proc. Natl. Acad. Sci. U.S.A.* **108**, 10098 (2011).
14. B. Wiedenheft *et al.*, *Proc. Natl. Acad. Sci. U.S.A.* **108**, 10092 (2011).
15. B. Wiedenheft *et al.*, *Nature* **477**, 486 (2011).
16. C. R. Hale *et al.*, *Cell* **139**, 945 (2009).
17. J. A. L. Howard, S. Delmas, I. Ivančić-Baće, E. L. Bolt, *Biochem. J.* **439**, 85 (2011).
18. E. R. Westra *et al.*, *Mol. Cell* **46**, 595 (2012).
19. C. R. Hale *et al.*, *Mol. Cell* **45**, 292 (2012).
20. J. Zhang *et al.*, *Mol. Cell* **45**, 303 (2012).
21. K. S. Makarova *et al.*, *Nat. Rev. Microbiol.* **9**, 467 (2011).
22. K. S. Makarova, N. V. Grishin, S. A. Shabalina, Y. I. Wolf, E. V. Koonin, *Biol. Direct* **1**, 7 (2006).
23. K. S. Makarova, L. Aravind, Y. I. Wolf, E. V. Koonin, *Biol. Direct* **6**, 38 (2011).
24. S. Gottesman, *Nature* **471**, 588 (2011).
25. R. Barrangou *et al.*, *Science* **315**, 1709 (2007).
26. J. E. Garneau *et al.*, *Nature* **468**, 67 (2010).
27. R. Sapranauskas *et al.*, *Nucleic Acids Res.* **39**, 9275 (2011).
28. G. K. Taylor, D. F. Heiter, S. Pietrokovski, B. L. Stoddard, *Nucleic Acids Res.* **39**, 9705 (2011).
29. H. Deveau *et al.*, *J. Bacteriol.* **190**, 1390 (2008).
30. B. P. Lewis, C. B. Burge, D. P. Bartel, *Cell* **120**, 15 (2005).
31. G. Hutvagner, M. J. Simard, *Nat. Rev. Mol. Cell Biol.* **9**, 22 (2008).
32. F. J. M. Mojica, C. Díez-Villaseñor, J. García-Martínez, C. Almendros, *Microbiology* **155**, 733 (2009).
33. L. A. Marraffini, E. J. Sontheimer, *Nature* **463**, 568 (2010).
34. D. G. Sashital, B. Wiedenheft, J. A. Doudna, *Mol. Cell* **46**, 606 (2012).
35. M. Christian *et al.*, *Genetics* **186**, 757 (2010).
36. J. C. Miller *et al.*, *Nat. Biotechnol.* **29**, 143 (2011).
37. F. D. Urnov, E. J. Rebar, M. C. Holmes, H. S. Zhang, P. D. Gregory, *Nat. Rev. Genet.* **11**, 636 (2010).
38. D. Carroll, *Gene Ther.* **15**, 1463 (2008).

Acknowledgments: We thank K. Zhou, A. M. Smith, R. Haurwitz and S. Sternberg for excellent technical assistance; members of the Doudna and Charpentier laboratories and J. Cate for comments on the manuscript; and B. Meyer and T.-W. Lo (Univ. of California, Berkeley/HHMI) for providing the GFP plasmid. This work was funded by the HHMI (M.J. and J.A.D.), the Austrian Science Fund (grant W1207-B09; K.C. and E.C.), the Univ. of Vienna (K.C.), the Swedish Research Council (grants K2010-57X-21436-01-3 and 621-2011-5752-LiMS; E.C.), the Kempe Foundation (E.C.), and Umeå University (K.C. and E.C.). J.A.D. is an Investigator and M.J. is a Research Specialist of the HHMI. K.C. is a fellow of the Austrian Doctoral Program in RNA Biology and is cosupervised by R. Schroeder. We thank A. Witte, U. Bläsi, and R. Schroeder for helpful discussions, financial support to K.C., and for hosting K.C. in their laboratories at MFPL. M.J., K.C., J.A.D., and E.C. have filed a related patent.

Supplementary Materials

www.sciencemag.org/cgi/content/full/science.1225829/DC1
Materials and Methods
Figs. S1 to S15
Tables S1 to S3
References (*39*–*47*)

8 June 2012; accepted 20 June 2012
Published online 28 June 2012;
10.1126/science.1225829

Long-Range Incommensurate Charge Fluctuations in (Y,Nd)$Ba_2Cu_3O_{6+x}$

G. Ghiringhelli,[1]* M. Le Tacon,[2] M. Minola,[1] S. Blanco-Canosa,[2] C. Mazzoli,[1] N. B. Brookes,[3] G. M. De Luca,[4] A. Frano,[2,5] D. G. Hawthorn,[6] F. He,[7] T. Loew,[2] M. Moretti Sala,[3] D. C. Peets,[2] M. Salluzzo,[4] E. Schierle,[5] R. Sutarto,[7,8] G. A. Sawatzky,[8] E. Weschke,[5] B. Keimer,[2]* L. Braicovich[1]

The concept that superconductivity competes with other orders in cuprate superconductors has become increasingly apparent, but obtaining direct evidence with bulk-sensitive probes is challenging. We have used resonant soft x-ray scattering to identify two-dimensional charge fluctuations with an incommensurate periodicity of ~3.2 lattice units in the copper-oxide planes of the superconductors (Y,Nd)$Ba_2Cu_3O_{6+x}$, with hole concentrations of 0.09 to 0.13 per planar Cu ion. The intensity and correlation length of the fluctuation signal increase strongly upon cooling down to the superconducting transition temperature (T_c); further cooling below T_c abruptly reverses the divergence of the charge correlations. In combination with earlier observations of a large gap in the spin excitation spectrum, these data indicate an incipient charge density wave instability that competes with superconductivity.

A successful theory of high-temperature superconductivity in the copper oxides requires a detailed understanding of the spin, charge, and orbital correlations in the normal state from which superconductivity emerges. In recent years, evidence of ordering phenomena in which these correlations might take on particularly simple forms has emerged (*1*, *2*). Despite intense efforts, however, only two order parameters other than superconductivity have thus far been unambiguously identified by bulk-sensitive experimental probes: (i) uniform antiferromagnetism in undoped insulating cuprates and (ii) uniaxially modulated antiferromagnetism (*3*) combined with charge order (*3*, *4*) in doped cuprates of the so-called "214" family [that is, compounds of composition $La_{2-x-y}(Sr,Ba)_x(Nd,Eu)_yCuO_4$]. The latter is known as "stripe order," with a commensurate charge modulation of period 4a (where lattice unit a = 3.8 to 3.9 Å is the distance between neighboring Cu atoms in the CuO_2 planes), which greatly reduces the superconducting transition temperature (T_c) of 214 materials at a doping level $p \sim 1/8$ per planar Cu atom. Incommensurate spin fluctuations in 214 materials with $p \neq 1/8$ (*5*) have been interpreted as evidence of fluctuating stripes (*6*). A long-standing debate has evolved around the questions of whether stripe order is a generic feature of the copper oxides and whether stripe fluctuations are essential for superconductivity.

Recent attention has focused on the "123" family [$RBa_2Cu_3O_{6+x}$ with R = Y or another rare earth element], which exhibits substantially lower chemical disorder and higher maximal T_c than the 214 system. For underdoped 123 compounds, the anomaly in the T_c-versus-p relation at $p = 1/8$ (*7*) and the large in-plane anisotropies in the transport properties (*8*, *9*) have been interpreted as evidence of stripe order or fluctuations, in analogy to stripe-ordered 214 materials (*10*). Differences in the spin dynamics of the two families have, however, cast some doubt on this interpretation. In particular, neutron-scattering studies of moderately doped 123 compounds have revealed a gap of magnitude ≥20 meV in the magnetic excitation spectrum (*11*–*14*), whereas 214 compounds with similar hole concentrations exhibit nearly gapless spin excitations (*5*). Further questions have been raised by the recent discovery of small Fermi surface pockets in quantum oscillation experiments on underdoped 123 materials in magnetic fields large enough to weaken or obliterate superconductivity (*15*). Some researchers have attributed this observation to a Fermi surface reconstruction due to magnetic field–induced stripe order (*10*), whereas others have argued that even the high magnetic fields applied in these experiments appear incapable of closing the spin gap and that a biaxial charge modulation is required to explain the quantum oscillation data (*16*). Nuclear magnetic resonance (NMR) experiments have shown evidence of a magnetic field–induced uniaxial charge modulation (*17*), but they do not yield information about electronic fluctuations outside of a very narrow energy window of ~1 μeV. On the other hand, scattering experiments to determine

[1]CNR-SPIN, Consorzio Nazionale Interuniversitario per le Scienze Fisiche della Materia, and Dipartimento di Fisica, Politecnico di Milano, Piazza Leonardo da Vinci 32, I-20133 Milano, Italy. [2]Max-Planck-Institut für Festkörperforschung, Heisenbergstraße 1, D-70569 Stuttgart, Germany. [3]European Synchrotron Radiation Facility (ESRF), BP 220, F-38043 Grenoble Cedex, France. [4]CNR-SPIN, Complesso Monte Sant'Angelo–Via Cinthia, I-80126 Napoli, Italy. [5]Helmholtz-Zentrum Berlin für Materialien und Energie, Albert-Einstein-Straße 15, D-12489 Berlin, Germany. [6]Department of Physics and Astronomy, University of Waterloo, Waterloo, Ontario N2L 3G1, Canada. [7]Canadian Light Source, University of Saskatchewan, Saskatoon, Saskatchewan S7N 0X4, Canada. [8]Department of Physics and Astronomy, University of British Columbia, Vancouver, British Columbia V6T 1Z4, Canada.

*To whom correspondence should be addressed. E-mail: giacomo.ghiringhelli@fisi.polimi.it (G.G.); b.keimer@fkf.mpg.de (B.K.)

the periodicity of this modulation and/or to characterize its spin or charge dynamics can currently not be performed under the extreme experimental conditions required to stabilize the high-field phase. Therefore, the nature of the leading electronic instability of doped 123 materials and its relation to superconductivity and to stripe order remain largely unknown.

Here, we report the results of resonant x-ray scattering (RXS) experiments especially designed to detect charge order and/or corresponding fluctuations on electronic energy scales. In contrast to earlier nonresonant x-ray scattering experiments on the same 123 compounds (*18*, *19*), the use of photons with energies near the Cu L_3 absorption edge ($2p_{3/2} \rightarrow 3d$ transitions, $h\nu \simeq 931$ eV) greatly enhances the sensitivity of the scattering signal to the valence electron system (*20*). The layered crystal structure of the 123 system (Fig. 1A) and the consequent two-dimensional (2D) scattering cross section (*20*) allow for easy variation of the momentum-transfer component parallel to the CuO_2 planes ($q_{//}$) through rotations of the sample at a fixed scattering angle (Fig. 1, B and C). Further experimental parameters include the energy of the incident photons and their polarization (Fig. 1B). Most of the measurements were carried out with a spectrometer, and the energy transferred by the photon was monitored with a combined instrumental resolution of ~130 meV. Unlike in conventional RXS, we could discriminate between the elastic and quasi-elastic signal coming from charge density fluctuations and the dominant inelastic contribution (Fig. 1D) (*21*, *22*).

Our central observation is apparent in the raw spectra of underdoped $Nd_{1+x}Ba_{2-x}Cu_3O_7$, shown in Fig. 1D as a function of both photon energy loss and $q_{//}$ along the (1,0) direction, parallel to the Cu-O bonds (Fig. 1B). The inelastic portion of the spectrum comprises features around 100 to 300 meV resulting from paramagnon excitations (*23*) and from 1 to 3 eV due to interorbital transitions (*dd* excitations) (*21*). These features depend weakly on $q_{//}$, whereas the response centered at zero energy loss exhibits a pronounced maximum at $q_{//} = (0.31,0)$. Scans around symmetry-equivalent, reciprocal-space points (*20*) on multiple samples (see below) have confirmed that the latter feature is generic to the 123 system and that its intensity maximum is at a wave vector distinctly different from the commensurate position (1/3,0). We will refer to this feature as a resonant elastic x-ray scattering (REXS) peak, although, as shown below, it arises from low-energy fluctuations of the valence-electron charge density in the CuO_2 planes and, hence, is not truly elastic.

The 123 structure contains copper atoms in two different crystallographic sites: (i) Cu2 atoms in the CuO_2 layers that are common to all high-temperature superconductors and (ii) Cu1 atoms in chains specific to the 123 system that act as charge reservoirs for the layers (Fig. 1A). In x-ray absorption (XAS) and RXS experiments, signals arising from Cu1 and Cu2 sites can be differentiated by virtue of their distinct absorption resonance energy and photon polarization dependence (Fig. 2C) (*24*). The anomalous REXS peak is present only when the photon energy is tuned to the $3d^9$ configuration of Cu2 sites (Fig. 2, D and E) and, hence, can be unambiguously assigned to the CuO_2 planes. Further confirmation for this assignment comes from a comparison of $q_{//}$ scans along the (0,1) and (1,0) directions (parallel and perpendicular to the chains, respectively) in untwinned $YBa_2Cu_3O_{6.6}$ crystals (Fig. 2A). The presence of equally intense REXS peaks in the two directions is incompatible with an origin in the Cu1 chains.

We now use the dependence of the RXS cross section on the polarization geometry to address the question of whether the REXS signal arises from a modulation of the charge or spin density in the CuO_2 layers. To separate these two scattering channels, we measured the scattering intensity for σ (Fig. 2A) and π polarization of the incident beam and for the two opposite directions of $q_{//}$ along (1,0) (Fig. 1C). In Fig. 2B, we compare the results to model calculations for spin-flip and non–spin-flip RXS from Cu2 sites with $3d^9(x^2 - y^2)$ ground-state symmetry (*25*, *26*). In contrast to the 100- to 300-meV loss feature, which follows the behavior expected for spin-flip scattering as seen before in undoped and doped cuprates (*22*, *23*), the polarization dependence of the REXS peak indicates that it arises from charge scattering.

Figure 3 provides an overview of the REXS response in a variety of different 123 samples, including both single crystals of $YBa_2Cu_3O_{6+x}$, where the doping level p is adjusted through the density and arrangement of oxygen atoms in the Cu1 chain layer, and thin films of $Nd_{1+x}Ba_{2-x}Cu_3O_7$, where the Cu1 chains are fully oxygenated and p is controlled through the Nd/Ba ratio. The presence of closely similar charge-fluctuation peaks

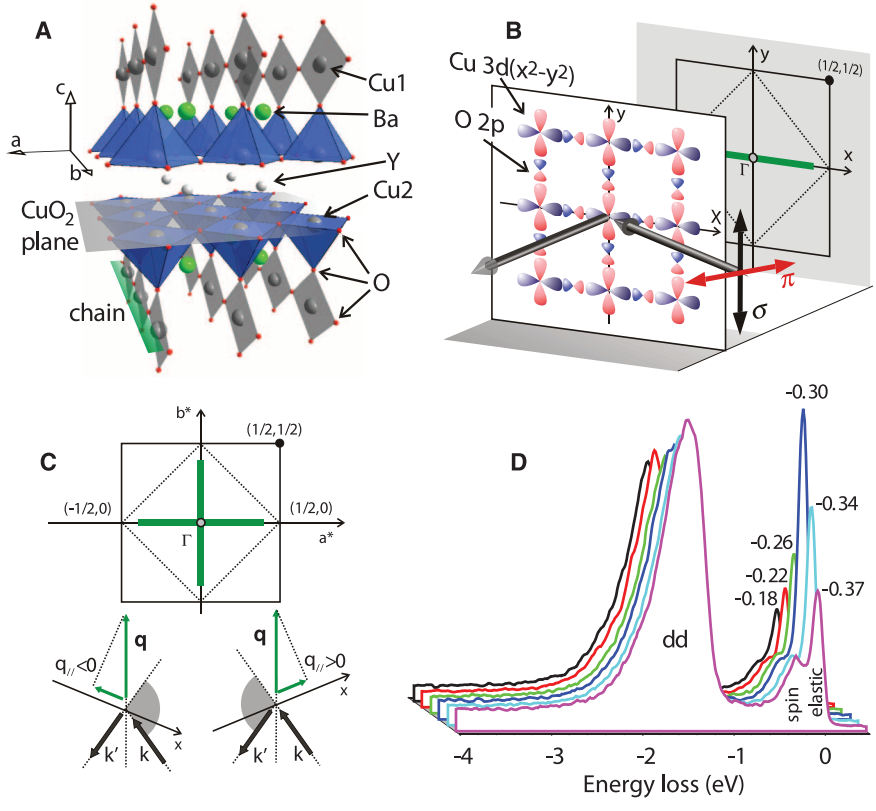

Fig. 1. Resonant soft x-ray scattering from layered cuprates. (**A**) Crystalline structure of $YBa_2Cu_3O_{6+x}$ superconductors. For $x < 1$, some of the O atoms along the chains are missing. (**B**) Scattering geometry with the c and either a or b axes in the scattering plane. The incident photon polarization can be parallel (π) or perpendicular (σ) to the scattering plane. The real and reciprocal spaces are sketched in the front and rear plane, respectively. In the real-space image, the Cu $3dx^2 - y^2$ and O $2p$ orbitals are shown. In the reciprocal-space image, the nuclear and magnetic first Brillouin zones are drawn with solid and dotted lines, respectively; the thick green line indicates the range covered by the experiments. Γ labels the (0,0) point, origin of the reciprocal space and center of the first Brillouin zone. (**C**) The in-plane component $q_{//}$ of the transferred momentum ranges from −0.4 to +0.4 rlu along the (1,0) or (0,1) direction when the sample is rotated around the y axis at a fixed scattering angle, indicated by the gray arcs (130° in most cases). (**D**) In the Cu L_3 energy-resolved RXS spectra of underdoped $Nd_{1.2}Ba_{1.8}Cu_3O_7$ (T_c = 65 K, T = 15 K, σ polarization), the quasi-elastic component has a maximum intensity at $q_{//} = -0.31$ rlu. The dispersing paramagnons (spin) are visible next to the quasi-elastic peak; the interorbital excitations (dd) around 2 eV carry most of the spectral weight.

at $|q_{\parallel}| \simeq 0.31$ reciprocal lattice units (rlu) in both systems in the range $0.09 \le p \le 0.13$ confirms that they are independent of the Cu1 chains and other details of the doping mechanism. Samples outside this narrow p range do not show any evidence of the anomalous REXS response, in agreement with earlier RXS work (*24*). This implies weaker charge fluctuations in samples at lower p, where incommensurate magnetic order has been observed at low temperatures (*27*), and at higher p, where the superconducting T_c is maximal. The range in which the REXS peak is observed coincides with the well-known plateau in the T_c-versus-p relation of the 123 system (shaded region in Fig. 3), which suggests that competition between superconducting and charge density correlations is responsible for the anomalously low T_c in this range.

To further explore the interplay between superconductivity and the anomalous charge density response, we have measured the temperature dependence of the REXS peak, both in the energy-resolved mode presented above and in the more traditional energy-integrated detection (Fig. 4, A and B). The peak is present both above and below the superconducting T_c. It narrows continuously upon cooling toward T_c, indicating a pronounced increase of the correlation length that reaches $(16 \pm 2)a$ at T_c of $YBa_2Cu_3O_{6.6}$, to be compared with domain sizes in the range of $40a$ to $66a$ for stripe-ordered $La_{1.875}Ba_{0.125}CuO_4$ (*4*, *28*, *29*). The T-dependent correlation length demonstrates that the signal arises from charge density fluctuations, rather than a static charge density wave (CDW). The incipient CDW phase transition heralded by the nearly diverging correlation length is preempted by the superconducting transition, which manifests itself in an abrupt decrease of the intensity and correlation length of the REXS peak (Fig. 4, C and D). This constitutes direct evidence of the competition between superconducting and incommensurate CDW states, which was already suggested by the doping dependence of the REXS response (Fig. 3). CDW correlations were previously observed by scanning

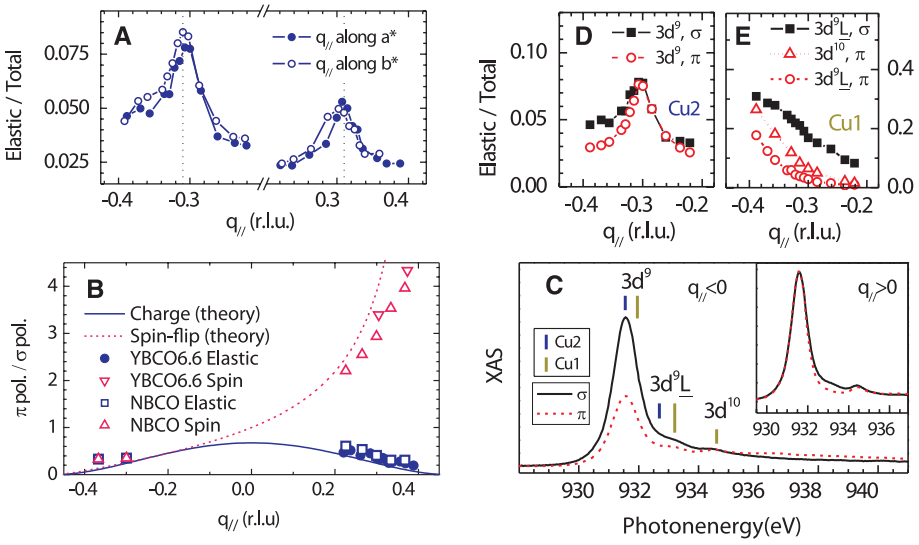

Fig. 2. Polarization and energy dependence of the REXS peak in $YBa_2Cu_3O_{6.6}$. (**A**) REXS scans measured at the Cu L_3 edge for positive and negative values of $q_{\parallel}$ along (1,0) and (0,1), using σ polarization (*20*). (**B**) Ratio between the REXS signal intensities obtained with π and σ polarizations (pol.). The experimental data for $YBa_2Cu_3O_{6.6}$ and $Nd_{1.2}Ba_{1.8}Cu_3O_7$ are compared to the model calculations (see text for details) and to the magnetic excitation signal (100- to 300-meV energy loss). (**C**) XAS spectra of $YBa_2Cu_3O_{6.6}$ with two polarizations and two geometries corresponding to negative and positive values of $q_{\parallel}$ (Fig. 1C). The main contributions to the XAS peaks are indicated. RXS with photon energies at the main absorption peak of 931.5 eV selects signals arising from the Cu2 sites. (**D** and **E**) REXS scans show the CDW peak only when exciting at the Cu2 sites and show nothing at higher excitation energies.

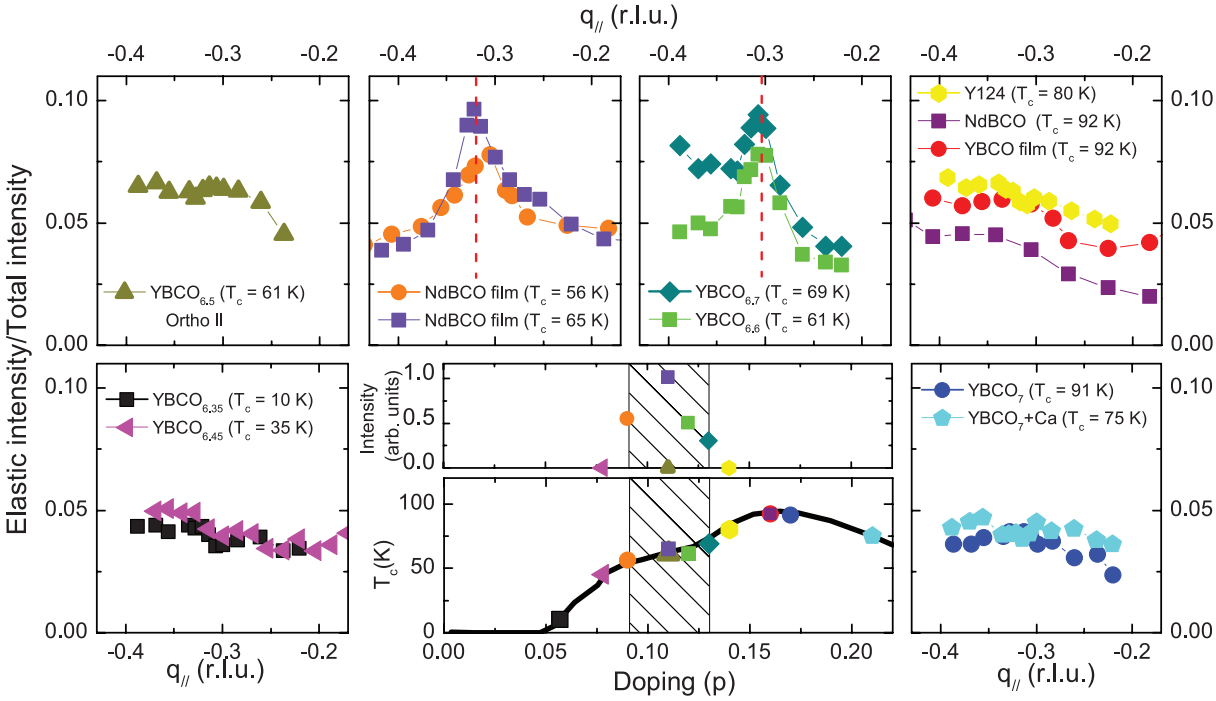

Fig. 3. Dependence of the CDW signal at 15 K on the hole doping level p. The CDW signal is present in several $YBa_2Cu_3O_{6+x}$ and $Nd_{1+y}Ba_{2-y}Cu_3O_7$ samples, but only for $0.09 \le p \le 0.13$. In this doping range (shaded in the central panel), the T_c-versus-p relation exhibits a plateau. The CDW peak position does not change with p outside of the experimental error, but its intensity is maximum at $p \simeq 0.11$.

tunneling spectroscopy (STS) on the surface of superconducting $Bi_2Sr_2CuO_{6+\delta}$ (2201) (*30*) and $Bi_2Sr_2CaCu_2O_{8+\delta}$ (2212) (*31*–*33*), but only limited information is available from STS on the temperature evolution of the CDW correlations in the 2201 and 2212 compounds, and the relation of the STS data to the superconducting properties in the bulk of these materials is obscured by electronic inhomogeneity.

The wave vector of the charge correlations revealed in our experiments is in good agreement with the nesting vector of the antibonding Fermi surface sheets predicted by density functional calculations for the 123 system (*34*). The nesting vector connects those segments on the 2D Fermi surface that develop the maximal gap amplitude in the *d*-wave superconducting state. The CDW is thus a natural consequence of a Fermi surface instability competing with superconductivity (*35*). The nearly critical nature of the charge fluctuations (Fig. 4) suggests a CDW ground state for underdoped 123 materials in magnetic fields sufficient to weaken or obliterate superconductivity, which may be responsible for the Fermi surface reconstruction evidenced by the quantum oscillation data (*15*). This scenario agrees qualitatively with a recent NMR study of $YBa_2Cu_3O_{6.5}$ in high magnetic fields, which has revealed signatures of a field-induced CDW (*17*), and with theoretical work on this issue (*16*, *36*). In this precise case, the long range ortho-II oxygen order and/or the high-field conditions may favor the uniaxial commensurate charge modulation with period 4*a* inferred from these data. Further work is required to understand the interplay between the chain order and the in-plane charge modulation and to reconcile our results with the NMR data.

It is instructive to compare the charge correlations revealed by our RXS experiments to the *p* evolution of the spin correlations previously determined by magnetic neutron scattering. For $p \leq 0.08$, these experiments revealed incommensurate magnetic order with wave vectors $q_{\parallel} = \left(\frac{1}{2} + \delta, \frac{1}{2}\right)$, where the incommensurability δ increases monotonically with *p* (*27*). Figure 3 shows that neither charge order nor low-energy incommensurate charge fluctuations are present in this doping range. For $p > 0.08$, the spin correlations remain centered at wave vectors similar to those at lower *p*, which bear no simple relation to the wave vector of the REXS peaks determined here (*11*–*14*). In this doping range, magnetic order disappears (*27*, *37*, *38*), and the magnetic excitation spectrum develops a large gap that increases smoothly with *p*, in stark contrast to the abrupt appearance and disappearance of the charge density correlations with increasing *p*.

These considerations imply that spin and charge order are decoupled in the 123 family, which is quite different from in the 214 family where they coexist microscopically in the striped state. The small or absent intensity difference between the signal intensities at $q_{//} = (0.31,0)$ and (0,0.31) (Fig. 2A) call into question the interpretation of various transport anomalies in the normal state of underdoped 123 compounds in terms of stripe fluctuations (*8*, *9*), at least in the doping range where we observed the REXS peaks. Although further experiments are required to establish whether these peaks arise from an equal distribution of fluctuating domains of two uniaxial CDWs with mutually perpendicular propagation vectors or from a single CDW with biaxial charge modulation, the isotropic intensity distribution of the CDW signal shows that these fluctuations cannot account for the strongly anisotropic resistivity and Nernst effect in the normal state. Despite these materials-specific variations, our data imply that long-range CDW correlations are a common feature of underdoped cuprates. Detailed microscopic calculations are required to assess their relation to the pseudogap phenomenon (*1*), the unusual $q = 0$ order (*39*), and the polar Kerr effect measurements (*40*) recently reported in some of these materials. The extensive *q*-, *p*-, and *T*-dependent data set we report here is an excellent basis for theoretical work on these issues.

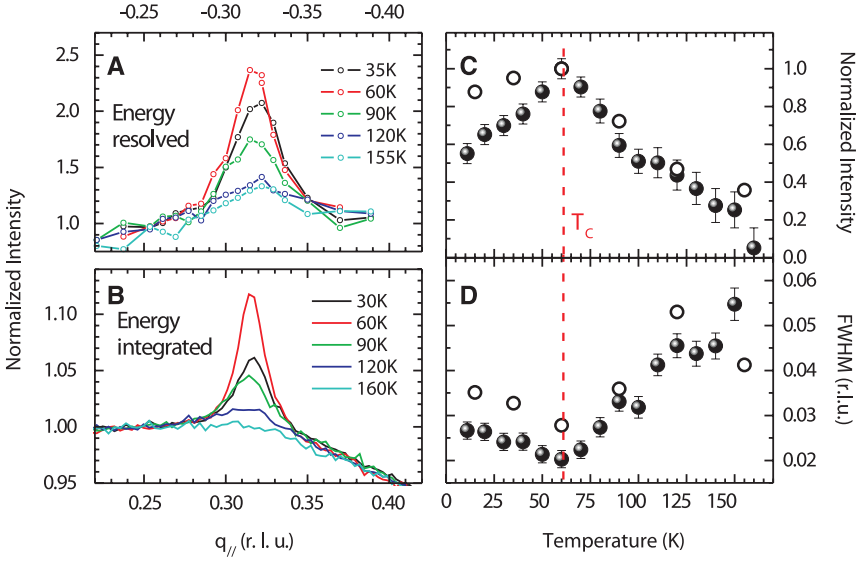

Fig. 4. Temperature dependence of the CDW signal in $YBa_2Cu_3O_{6.6}$. (**A** and **B**) Comparison of RXS scans at selected temperatures, as obtained with an energy-resolving instrument and with a conventional diffractometer for soft x-rays. (**C** and **D**) *T*-dependence of the CDW intensity and full width at half maximum (FWHM) derived from the energy-resolved (open circles) and the energy-integrated data (solid circles) for σ polarization.

References and Notes

1. M. Vojta, *Adv. Phys.* **58**, 699 (2009).
2. R.-H. He *et al.*, *Science* **331**, 1579 (2011).
3. J. M. Tranquada, B. J. Sternlieb, J. D. Axe, Y. Nakamura, S. Uchida, *Nature* **375**, 561 (1995).
4. P. Abbamonte *et al.*, *Nat. Phys.* **1**, 155 (2005).
5. R. J. Birgeneau, C. Stock, J. M. Tranquada, K. Yamada, *J. Phys. Soc. Jpn.* **75**, 111003 (2006).
6. S. A. Kivelson *et al.*, *Rev. Mod. Phys.* **75**, 1201 (2003).
7. R. Liang, D. A. Bonn, W. N. Hardy, *Phys. Rev. B* **73**, 180505 (2006).
8. X. F. Sun, K. Segawa, Y. Ando, *Phys. Rev. Lett.* **93**, 107001 (2004).
9. R. Daou *et al.*, *Nature* **463**, 519 (2010).
10. F. Laliberté *et al.*, *Nat. Commun.* **2**, 432 (2011).
11. H. F. Fong *et al.*, *Phys. Rev. B* **61**, 14773 (2000).
12. P. C. Dai, H. A. Mook, R. D. Hunt, F. Dogan, *Phys. Rev. B* **63**, 054525 (2001).
13. C. Stock *et al.*, *Phys. Rev. B* **71**, 024522 (2005).
14. V. Hinkov *et al.*, *Nat. Phys.* **3**, 780 (2007).
15. N. Doiron-Leyraud *et al.*, *Nature* **447**, 565 (2007).
16. N. Harrison, S. E. Sebastian, *Phys. Rev. Lett.* **106**, 226402 (2011).
17. T. Wu *et al.*, *Nature* **477**, 191 (2011).
18. N. H. Andersen *et al.*, *Physica C* **317–318**, 259 (1999).
19. J. Strempfer *et al.*, *Phys. Rev. Lett.* **93**, 157007 (2004).
20. Materials and methods are available as supplementary materials on *Science* Online.
21. G. Ghiringhelli *et al.*, *Phys. Rev. Lett.* **92**, 117406 (2004).
22. L. Braicovich *et al.*, *Phys. Rev. Lett.* **104**, 077002 (2010).
23. M. Le Tacon *et al.*, *Nat. Phys.* **7**, 725 (2011).
24. D. G. Hawthorn *et al.*, *Phys. Rev. B* **84**, 075125 (2011).
25. L. J. P. Ament, G. Ghiringhelli, M. M. Sala, L. Braicovich, J. van den Brink, *Phys. Rev. Lett.* **103**, 117003 (2009).
26. M. Moretti Sala *et al.*, *New J. Phys.* **13**, 043026 (2011).
27. D. Haug *et al.*, *New J. Phys.* **12**, 105006 (2010).
28. S. B. Wilkins *et al.*, *Phys. Rev. B* **84**, 195101 (2011).
29. M. Hücker *et al.*, *Phys. Rev. B* **83**, 104506 (2011).
30. W. D. Wise *et al.*, *Nat. Phys.* **4**, 696 (2008).
31. J. E. Hoffman *et al.*, *Science* **295**, 466 (2002).
32. C. Howald, H. Eisaki, N. Kaneko, M. Greven, A. Kapitulnik, *Phys. Rev. B* **67**, 014533 (2003).
33. C. V. Parker *et al.*, *Nature* **468**, 677 (2010).
34. O. K. Andersen *et al.*, *Physica C* **185-189**, 147 (1991).
35. C. Castellani, C. Di Castro, M. Grilli, *Phys. Rev. Lett.* **95**, 4650 (1995).
36. H. Yao, D.-H. Lee, S. A. Kivelson, *Phys. Rev. B* **84**, 012507 (2011).
37. F. Coneri, S. Sanna, K. Zheng, J. Lord, R. De Renzi, *Phys. Rev. B* **81**, 104507 (2010).
38. A. Rigamonti, F. Borsa, P. Carretta, *Rep. Prog. Phys.* **61**, 1367 (1998).

39. B. Fauqué *et al.*, *Phys. Rev. Lett.* **96**, 197001 (2006).
40. J. Xia *et al.*, *Phys. Rev. Lett.* **100**, 127002 (2008).

Acknowledgments: This work was performed partly at the Advanced Resonant Spectroscopies (ADRESS) beamline of the Swiss Light Source, using the Super Advanced X-ray Emission Spectrometer (SAXES) instrument jointly built by Paul Scherrer Institut (Villigen, Switzerland), Politecnico di Milano (Italy), and École Polytechnique Fédérale de Lausanne (Switzerland); partly at the ID08 beam line of the ESRF (Grenoble, France); partly at the UE46-PGM1 beamline of Bessy-II (Helmholtz-Zentrum Berlin für Materialien und Energie, Germany); and partly at the Resonant Elastic and Inelastic X-ray Scattering (REIXS) beamine at the Canadian Light Source (CLS; Saskatoon, Saskatchewan, Canada). Part of this research project has been supported by the European Commission under the 7th Framework Programme: Research Infrastructures (grant agreement number 226716), the European project "SOPRANO" under Marie Curie actions (grant no. PITNGA-2008-214040), the German Science Foundation under SFB/TRR 80, and by the Italian Ministry of Research [Ministero dell'Istruzione, Università e Ricerca (MIUR), grant no. PRIN-20094W2LAY]. The research at the CLS is supported by the Natural Sciences and Engineering Research Council of Canada, the National Research Council, the Canadian Institutes of Health Research, and the Univ. of Saskatchewan. We gratefully thank S. Kivelson, T. Devereaux, S. Sebastian, M.-H. Julien, and G. Khaliullin for discussions; T. Schmitt, K. Zhou, and C. Monney for support at the ADRESS beamline; and V. Hinkov, C. Lin, M. Bakr, M. Raichle, and D. Haug for preparation of some of the single-crystal samples. M.S. acknowledges additional funding from the CNR Institute and from the European Union Community.

Supplementary Materials
www.sciencemag.org/cgi/content/full/science.1223532/DC1
Materials and Methods
Figs. S1 to S4
Table S1
References (*41*–*51*)

18 April 2012; accepted 2 July 2012
Published online 12 July 2012;
10.1126/science.1223532

Long-Range Ordered Carbon Clusters: A Crystalline Material with Amorphous Building Blocks

Lin Wang,[1,2]* Bingbing Liu,[2] Hui Li,[3] Wenge Yang,[1] Yang Ding,[4] Stanislav V. Sinogeikin,[5] Yue Meng,[5] Zhenxian Liu,[6] Xiao Cheng Zeng,[3] Wendy L. Mao[7,8]

Solid-state materials can be categorized by their structures into crystalline (having periodic translation symmetry), amorphous (no periodic and orientational symmetry), and quasi-crystalline (having orientational but not periodic translation symmetry) phases. Hybridization of crystalline and amorphous structures at the atomic level has not been experimentally observed. We report the discovery of a long-range ordered material constructed from units of amorphous carbon clusters that was synthesized by compressing solvated fullerenes. Using x-ray diffraction, Raman spectroscopy, and quantum molecular dynamics simulation, we observed that, although carbon-60 cages were crushed and became amorphous, the solvent molecules remained intact, playing a crucial role in maintaining the long-range periodicity. Once formed, the high-pressure phase is quenchable back to ambient conditions and is ultra-incompressible, with the ability to indent diamond.

Carbon materials—such as graphene, graphite, diamond, fullerenes, and carbon nanotubes, as well as nanostructured and amorphous carbon—display a remarkable range of mechanical, electronic, and electrochemical properties that have led to many advanced applications (*1*–*7*). The structures of all of these materials are either ordered (crystalline) or disordered (amorphous). Polymeric fullerenes have been synthesized at different pressures and temperatures when pure C_{60} or C_{70} were used as starting materials (*8*–*11*). Under cold (ambient temperature) compression, the C_{60} cages collapse, and the crystalline C_{60} phase transforms into amorphous carbon above 30 GPa (*12*, *13*). Under high-temperature compression, pure C_{60} forms different polymerized structures, with the C_{60} cages transforming into graphitic carbon or a mixture of sp^2 and sp^3 amorphous phases. Some of these phases are also ultrahard (*8*, *11*, *14*, *15*).

Another type of starting material, solvated C_{60}, which is composed of C_{60} molecules separated by solvent molecules, has received considerable attention (*16*–*18*). The solvated fullerenes are crystalline materials with high stability, tunable metrics, and functionality. The incorporation of guest molecules into the host C_{60} lattice changes the crystal structure. The changes are also reflected in their vibrational properties and, consequently, the Raman and IR (infrared absorption) spectra (*19*). It was reported that the guest molecules can hinder the rotation of the C_{60} molecules, leading to a decrease in their vibrational-rotational couplings (*20*, *21*). Furthermore, the interactions between C_{60} and the guest molecules reduce the icosahedral symmetry of the C_{60} molecules, allowing electronic transitions that are forbidden in pristine C_{60} and inducing a strong photoluminescent response (*22*).

C_{60}**m*-xylene, an important solvated C_{60} with greatly enhanced photon luminescence (*18*, *22*), was selected for this investigation. It was studied up to 60 GPa by using a diamond anvil cell. X-ray diffraction (XRD), Raman spectroscopy, infrared absorption spectroscopy, and inelastic x-ray scattering (IXS, also called x-ray Raman spectroscopy) were used to analyze the crystal structure, lattice vibration, and bonding type of the material at high pressures. Independent quantum molecular dynamics (QMD) simulations were also carried out to understand and provide insight into the phase transformation of the material under high pressure.

We used XRD to reveal long-range structural order. Detailed information about the experiments is shown in the supplementary materials. Typical XRD patterns of the C_{60}**m*-xylene during compression are shown in Fig. 1. The XRD pattern at ambient pressure is well indexed as individual C_{60} molecules occupying the lattice points of a hexagonal close-packed (hcp) structure (space group $P6_3$) with lattice constants a = 2.3761 nm and c = 1.0120 nm, in good agreement with literature values (*18*, *22*, *23*). During compression up to 60.1 GPa, the diffraction peaks gradually broaden, weaken, and shift to higher Q (reciprocal lattice vector). No drastic change was observed, indicating that the hcp periodicity of the molecules

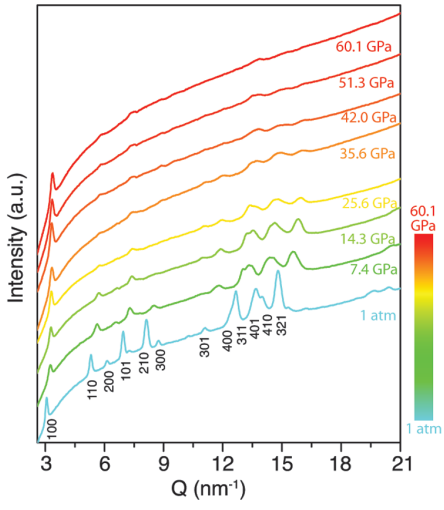

Fig. 1. XRD patterns of C_{60}**m*-xylene at different pressures. The numbers below the 1-atm XRD pattern indicate the indexing for the hcp structure. The pressures for the XRD patterns are given by the colored numbers at the right and in the bar.

[1]High Pressure Synergetic Consortium (HPSynC), Geophysical Laboratory, Carnegie Institution of Washington, Argonne, IL 60439, USA. [2]State Key Laboratory of Superhard Materials, Jilin University, Changchun 130012, China. [3]Department of Chemistry, University of Nebraska, Lincoln, NE 68588, USA. [4]Advanced Photon Source, Argonne National Laboratory, Argonne, IL 60439, USA. [5]High Pressure Collaborative Access Team (HPCAT), Geophysical Laboratory, Carnegie Institution of Washington, Argonne, IL 60439, USA. [6]Geophysical Laboratory, Carnegie Institution of Washington, Washington, DC 20015, USA. [7]Geological and Environmental Sciences, Stanford University, Stanford, CA 94305, USA. [8]Photon Science and Stanford Institute for Materials and Energy Sciences, SLAC National Accelerator Laboratory, Menlo Park, CA 94025, USA.

*To whom correspondence should be addressed. E-mail: lwang@ciw.edu